

A Hybrid Switched Reactive-Based Visual Servo Control of 5-DOF Robot Manipulators for Pick-and-Place Tasks

Chi-Yi Tsai, Ching-Chang Wong, Chia-Jun Yu, Chih-Cheng Liu, and Tsung-Yen Liu

Abstract—This paper addresses the problem of visual servo control for a five-degree-of-freedom robot manipulator to perform pick-and-place tasks. A new hybrid switched reactive-based visual servo control structure, inspired from a sensing-and-reaction behavior without the inverse interaction matrix computing, is proposed to handle this problem efficiently. The proposed structure is similar to the logic-based approaches, but the requirements of the fuzzy modeling and/or the fuzzy-rule base learning are omitted. To achieve this, a novel hardware-aware reactive function approach is presented to directly map an image position error vector to a desired end-effector velocity vector under the consideration of hardware limitations. This approach helps to simplify the implementation of visual servo systems with improved reliability. Moreover, the proposed control system is a hybrid switching controller consisting of both image-based and position-based reactive planning schemes, which allows improving the robustness and effectiveness of the visual servo system. Experimental results validate the performance of the proposed visual servo control method in a realistic scenario setting.

Index Terms—Hardware-aware reactive function, pick-and-place manipulation, reactive-based control, robot manipulator, visual servo control.

I. INTRODUCTION

IN the past two decades, robot manipulators have been widely applied in several industrial environments for autonomous manipulation tasks. In order for the robot to accomplish a variety of industrial applications, pick-and-place operation is one of the major requirements in autonomous robot manipulation. Such a requirement carried out many studies on robotic grasping control that traditionally can be divided into geometrical-planning-based and sensory-based approaches [1]. However, the traditional robotic grasping control approaches may fail due to uncertainties in either the end-effector pose or the object pose [2]. To improve the robustness of robotic grasping control system, vision sensor provides an effective solution to deal with pose uncertainties as visual sensing offers rich information on target object for feedback. This advantage continues to gain increasing attention on the research of vision-based grasping control in recent years. A generic vision-based

grasping control is broadly composed of three subprocesses. The first is object-of-interest extraction, which is an image process function involving object foreground/background segmentation, object detection, and object recognition. The second is vision-based grasp planning, which consists of object pose estimation, grasp point determination, and gripper motion planning. The last is vision-based pick-and-place control relying on techniques from visual servo control. These three subprocesses have been individually addressed in the literature, and this paper focuses the discussion on the last subprocess.

Industrial robotic manipulators usually employ visual servo control to autonomously grasp and manipulate various types of objects of interest in a more robust manner [3]. Modern visual servo control schemes can be classified into image-based, position-based, and advanced approaches [4]–[6]. These visual servoing schemes often require deriving a robot–target interaction matrix related between image features and robot kinematics. However, deriving the interaction matrix is not a trivial problem, particularly for an uncalibrated visual servo system. Moreover, the interaction matrix is related to the depth value of each image feature point relative to the camera frame, which is difficult to be measured when using a monocular vision system. Therefore, many advanced visual servoing schemes require employing an estimation process to estimate the depth value of each visual feature or interaction matrix of current camera–target configuration. This requirement leads to a more demanding vision and estimation design for a visual servo control system.

An alternative way to achieve robotic visual servo control is inspired from the behavior of living animals; for instance, human beings only see and grasp an object of interest without precise numerical interaction dynamics and position information. This biological inspiration leads to a completely different approach to realize visual servoing with only vision information [7]–[15]. In [7], Suh and Kim proposed a new type of interaction matrix, in which each element was associated with only the image features. A fuzzy controller with a supervised learning capability was then proposed to approximate a nonlinear mapping between feature variation and camera motion related to the new type of interaction matrix. The authors also extended their work to robot manipulation control via a fuzzy-membership-function-based neural network approximating the nonlinear mapping they discovered [8]. Although this method provides a good approximation on the mapping between feature variation and camera motion, the visual servo controller still requires computing an inverse of the approximate interaction matrix to determine each joint angle command. To fully avoid the computation of inverse interaction matrix, Sequeira Gonçalves *et al.* employed fuzzy modeling techniques to obtain an inverse model of the mapping between feature variations and

Manuscript received October 31, 2012; revised March 22, 2013, September 10, 2013, December 16, 2013, and January 26, 2014; accepted February 15, 2014. Date of publication October 13, 2014; date of current version March 2, 2015. This work was supported in part by the National Science Council of China under Contract NSC 102-2221-E-032-050 and Contract NSC 100-2622-E-032-003-CC3.

The authors are with the Department of Electrical Engineering, Tamkang University, Taipei 25137, Taiwan (e-mail: chi-yi_tsai@mail.tku.edu.tw; wong@ee.tku.edu.tw).

Color versions of one or more of the figures in this paper are available online at <http://ieeexplore.ieee.org>.

Digital Object Identifier 10.1109/JSYST.2014.2358876

joint velocities [9]. This approach provides an efficient way to obtain the inverse interaction matrix online; however, only an uncalibrated eye-to-hand visual servo system is addressed. Recently, the authors in [10] have proposed a distributed fuzzy proportional controller that adopts a Takagi–Sugeno (TS) fuzzy model [16] to estimate the inverse interaction matrix of the visual servo system. This method has been applied in an uncalibrated eye-in-hand robotic manipulator to show the estimation performance of the proposed TS fuzzy model. However, training the proposed TS fuzzy model requires constructing an analytical image-based visual servo controller to collect training data for learning process. This requirement decreases the applicability of the TS fuzzy modeling approach.

On the other hand, some researchers used fuzzy logic control techniques to achieve visual servo control without computing the inverse interaction matrix. Giuseppe *et al.* proposed a fuzzy reactive control scheme to imitate a sensing-and-reaction behavior for real-time grasping control of a three-degree-of-freedom (3-DOF) industrial manipulator [11]. Since this approach uses a monocular vision system with eye-in-hand structure, only grasping a spherical object of known size is addressed. To achieve more flexible robot manipulation control, Moreno-Armendariz and Yu proposed a fuzzy visual controller combined with a stereo vision system [12]. The stereo vision system first generates a desired 3-D end-effector position, and the fuzzy controller then controls the robot manipulator reaching the desired position. Recently, Bueno-López and Arteaga-Pérez extended this work to a 3-D trajectory tracking control scenario, but using a different stereo vision model [13]. Using fuzzy-logic-based approaches gains a benefit to avoid the training process required in fuzzy-modeling-based approaches; however, the fuzzy rules and membership functions of the fuzzy controller are still built in a supervised way. Although there exist some adaptive fuzzy control techniques for self-tuning fuzzy rules [14] or internal parameters of membership functions [15], the fuzzy visual servo controller of a 6-DOF robot manipulator usually requires designing at least three fuzzy controllers with different fuzzy behaviors to control three joint angles of the manipulator individually. Therefore, the design of self-tuning algorithm for multiple fuzzy controllers will become difficult when controlling more than three joint angles.

This paper describes the design, implementation, and verification of a practical visual servo control system for a 5-DOF robot manipulator to handle pick-and-place tasks. The proposed visual servoing scheme is also inspired from the sensing-and-reaction behavior, but completely different to the fuzzy-logic-based approaches. The proposed visual servo system is a hybrid switching control architecture consisting of image- and position-based visual servoing approaches, but it adopts a reactive-based control strategy to calculate the end-effector velocities using only vision information without inverse interaction matrix computing, fuzzy modeling, and fuzzy-rule base learning. The proposed visual reactive method is applied in a straightforward manner to map an image position error vector to a desired end-effector velocity vector. Each joint angle of the robot manipulator is then calculated from the desired end-effector positions via a conventional inverse kinematics controller [17]. The contribution of this work is summarized as follows.

- 1) A hybrid switched reactive-based visual servoing is proposed to integrate image- and position-based visual servoing schemes into a variable structure framework

without using interaction matrix, fuzzy modeling, or fuzzy-rule base. The proposed controller uses image-based visual servoing (IBVS) to grasp an object of interest nearby the gripper and uses position-based visual servoing (PBVS) to manipulate the grasped object. According to [5], IBVS is robust to errors in camera calibration and image noise, but the camera motion may follow a suboptimal Cartesian trajectory. By contrast, PBVS allows the camera to follow theoretically an optimal Cartesian trajectory. Therefore, the proposed hybrid switched reactive-based visual servoing scheme is beneficial to improving the robustness and effectiveness of the visual servoing system.

- 2) As to IBVS, a new image-based object orientation estimation is proposed to estimate the orientation of a geometric polygon object, such as a cubic object, randomly placed on a flat working table. This algorithm helps the robot manipulator to accurately grasp a geometric polygon object using vision information only.
- 3) A novel hardware-aware reactive function approach is presented to directly map the image position or world position errors to the desired end-effector velocities under the consideration of hardware limitations, such as system quantization uncertainties. This reactive-based approach allows simplifying the design of visual servo systems with improved reliability and applicability.

The remainder of this paper is organized as follows. Section II describes the scenario under consideration in this paper. Section III presents the design of the proposed image-based object orientation estimation algorithm that provides necessary information related to object orientation required in the following reactive control process. The proposed visual servo control approach is introduced in Section IV. Section V reports several experimental results to validate the performance of the developed visual servo control system. Finally, Section VI concludes the contributions of this work.

II. SCENARIO DESCRIPTION

This section describes the scenario considered in this paper. A 5-DOF robot manipulator aims to grasp a colored object and place it into a box, which has two different shapes of holes with different colors. The robot has to recognize the color and shape of the object of interest and try to put it into one of the boxes through a hole with the same color and shape. We first present the experimental setup for this scenario, and the robot manipulator is then introduced to perform pick-and-place tasks.

A. Experimental Setup

Fig. 1(a) shows the experimental setup in our scenario. As aforementioned, the robot manipulator is set up in front of a working table, where several color objects and four boxes are placed for the robot to perform the pick-and-place task. Fig. 1(b) illustrates the box used in the experiment. Each box has two holes with different colors and shapes, i.e., a spherical hole located at the inclined plane and a square one on the top of the box. Fig. 1(c) shows two types of color objects used in this scenario: the first one is a spherical-type object, and the second one is a cubic-type object. Each type of objects has four colors: red, green, blue, and yellow. Before performing the picking task, the robot first has to recognize the type and color of each object randomly placed on the table. To achieve

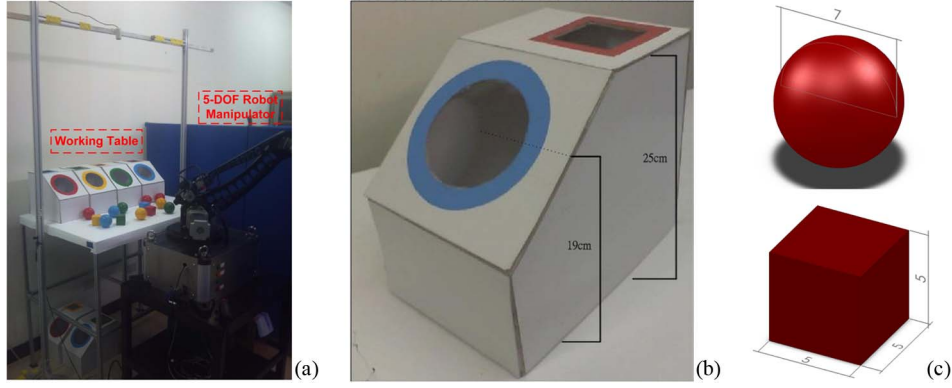


Fig. 1. (a) Scenario under consideration. (b) Box used in this scenario. Each box has two holes with different colors and shapes. (c) Two types of color objects used in this scenario.

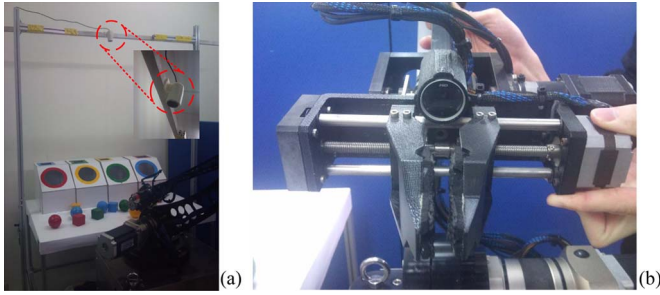


Fig. 2. Setup of the two cameras used in the experiments. (a) Camera mounted overhead the working table. (b) Camera mounted on the robot gripper.

this, a camera is mounted overhead [see Fig. 2(a)] to capture all objects and boxes placed on the table. A color segmentation algorithm and a support vector machine (SVM)-based shape classifier [18] are then applied to extract and classify these objects. After recognizing each object on the table, the robot manipulator performs local object picking task using the other camera mounted on its gripper [see Fig. 2(b)]. Note that the gripper-mounted camera only observes local objects of interest near the robot gripper and cannot observe the location of each hole at the same time. In this situation, the overhead mounted camera is able to provide the target location for the robot accomplishing the visual pick-and-place task.

Fig. 3 shows the hardware of the 5-DOF robot manipulator used in this study. The robot manipulator includes eight parts: (a) a base joint, (b) a shoulder joint, (c) a lower arm, (d) an elbow joint, (e) an upper arm, (f) a wrist joint, (g) a wrist rotation joint, and (h) a parallel jaw gripper. For each joint of the manipulator, a step motor with a gearbox is used as the joint motor so that each joint angle of the robot can rotate with a fixed degree when receiving a pulse signal from a motor driver [19]. As to the design of motion control card, an Altera DE0 development board [20] is employed to receive joint angle commands from a high-level controller (i.e., the proposed visual servo controller) and send control signals (a pulse train [21]) of each joint angle to the corresponding motor driver, which is able to transform the control signals into the pulse signals to drive a step motor.

In the gripper design, a screw with positive and negative threads is designed so that only one step motor is used for the gripper to grasp the object. Moreover, the mechanism of the parallel jaw gripper is designed to allow the robot grasping different types of objects, which helps to simplify the grasp planning design (i.e., omitting the grasping-point detection process).

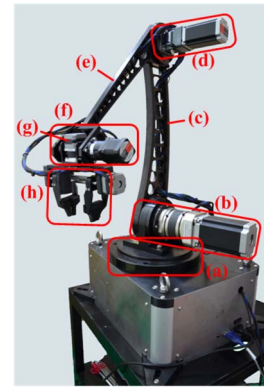


Fig. 3. Hardware of the 5-DOF robot manipulator used in the object pick-and-place experiments.

B. System Framework

Fig. 4 shows the system framework of the proposed visual servo control design, which is a hybrid switching architecture consisting of an image-based reactive planning unit, a position-based reactive planning unit, and an inverse kinematics controller. As mentioned in the previous subsection, the system requires two cameras to accomplish the object pick-and-place task that contains three stages. In the first stage, the overhead-mounted camera estimates the target center position in world coordinate to assist the position-based reactive planning process. The camera first captures the image of whole view of the table, and a color-based image segmentation algorithm is then applied to extract all color objects in the global observed image. Next, an SVM-based shape classifier is employed to classify all extracted color objects into four types of shape: spherical, cubic, spherical hole, and square hole. Based on these classified results, a coordinate conversion approach based on the conventional camera calibration techniques is adopted to convert the center position of all spherical-hole and square-hole objects from image coordinate to world coordinate. The converted coordinates will be used as the desired end-effector positions in world coordinate for the robot to put a grasped object. Moreover, the orientation of each square-hole is also estimated via an image-based object orientation estimation algorithm, which will be presented in Section III.

In the second stage, the gripper-mounted camera observes local objects near the gripper and provides their center positions in image coordinate to assist the image-based reactive planning process. The same color-based image segmentation and

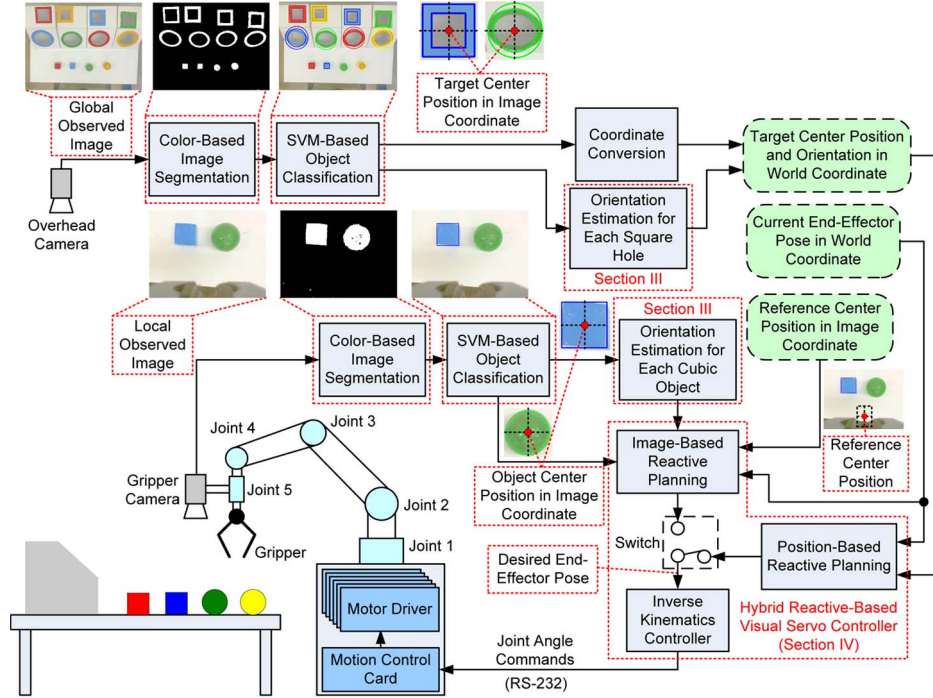


Fig. 4. System framework of the proposed visual servo control approach.

SVM-based shape classification processes used in the first stage are also employed in this stage to extract and classify all color objects in the local observed image. If one or more cubic objects are detected, the orientation of each cubic object is then estimated by using the proposed image-based object orientation estimation algorithm. Next, the proposed image-based reactive planning process determines the desired end-effector pose in world coordinate according to the difference between the reference and observed object center positions in image coordinate and the orientation information if grasping a cubic object.

In the final stage, two different control strategies, i.e., IBVS and PBVS, are used for picking and placing objects, respectively. The robot first performs IBVS: the inverse kinematics controller selects the desired end-effector pose generated from the image-based reactive planning to pick a local object of interest. When the robot picked the object, it then switches to PBVS: the inverse kinematics controller selects the desired end-effector pose generated from the position-based reactive planning to place the picked object into a corresponding hole with the same color and shape. The details of the proposed hybrid switched reactive-based visual servo controller will be presented in Section IV.

C. Available Assumptions

Since the proposed system is based entirely upon visual-sensing data, some assumptions about the cameras should be given. Based on the experimental setup discussed above, the following assumptions are noted with respect to the cameras.

(A1) *The optical axis of both cameras is perpendicular to the working table.* To estimate the orientation of both cubic and square-hole objects from the visual information, it is necessary that the camera optical axis is perpendicular to the plane where both objects lie. Since both cameras are fixed mounted on the steel stand and the end-effector, respectively, this assumption is achievable by designing a perpendicular camera steady on the steel stand for the

overhead-mounted camera and maintaining the pose of the end-effector perpendicular to the plane for the gripper-mounted camera.

(A2) *The focal lengths of both cameras are fixed during visual pick-and-place task.* This assumption can be achieved by disabling the autofocus function for each camera.

III. IMAGE-BASED OBJECT ORIENTATION ESTIMATION ALGORITHM

As mentioned in the previous section, to put a cubic object passing through a square hole, the robot first needs to estimate the orientation of the object and then turns it to the same orientation as the hole. Provided Assumption (A1), a well-known algorithm relying only upon visual information to achieve this purpose is based on the image moments [22]. Fig. 5(a) illustrates the orientation of a cubic object defined in this study (the angle θ_c in the figure). According to [22], the image-moments-based approach estimates the angle θ_c by the orientation of an equivalent ellipse with the same two-order centered moments as the object. This approach works well for an arbitrary object; however, it may fail to estimate the orientation of a regular polygon object (i.e., the cubic object considered here) since the corresponding equivalent ellipse is close to a circle. This problem highlights the importance of orientation estimation problem for the regular polygon objects. This section hence presents a novel image-based object orientation estimation algorithm that efficiently and accurately estimates the orientation of a geometric polygon object from a segmented image.

Let h be the height of an image patch containing a single cubic object. We first consider a boundary-point set $\Omega_B = \{\mathbf{p}_1^B, \mathbf{p}_2^B, \dots, \mathbf{p}_m^B\}$, where $\mathbf{p}_j^B = [u_j^B (h-1) - v_j^B]^T$ is associated with the boundary pixel $[u_j^B \ v_j^B]^T$ for $j = 1 \sim m$, of the cubic object in the image patch. Note that each boundary point

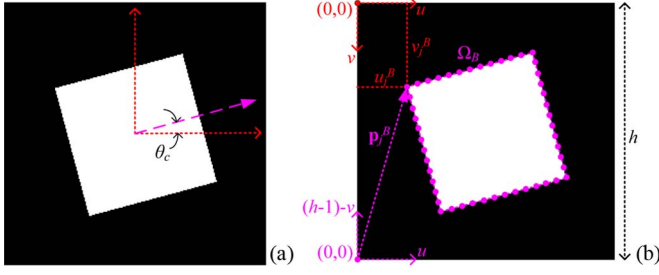


Fig. 5. Illustration of definitions used in this study. (a) and (b) Orientation and boundary-point set of a cubic object, respectively. Here, each boundary-point p_i^B takes the point $(0, h - 1)$ as the origin, not the origin of image patch.

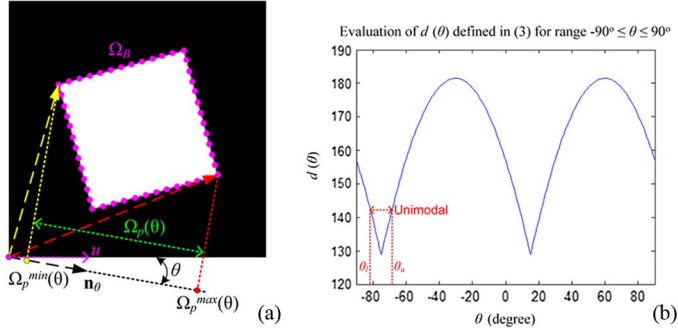


Fig. 6. Concept of the proposed orientation estimation method. (a) Projection-point set $\Omega_p(\theta)$ associated with a given unit vector \mathbf{n}_θ and a boundary-point set Ω_B . (b) Evaluation of the positive real-valued function defined in (3).

p_j^B can be seen as a 2-D vector taking the point $(0, h - 1)$ as the origin [see Fig. 5(b)]. Next, let \mathbf{n}_θ be a unit vector parameterized by a given angle θ such that

$$\mathbf{n}_\theta = [\cos \theta \quad \sin \theta]^T. \quad (1)$$

Based on (1), we define a projection-point set $\Omega_p(\theta)$ associated with a given unit vector \mathbf{n}_θ and a boundary-point set Ω_B such that

$$\Omega_p(\theta) = \{\mathbf{p}^T \mathbf{n}_\theta : \mathbf{p} \in \Omega_B\} \quad (2)$$

which is a real inner product space defined by the projection of the boundary-point set Ω_B onto the unit vector \mathbf{n}_θ , as shown in Fig. 6(a). Since the boundary-point set is bounded without loss of generality, the projection-point set is also bounded and closed so that $\Omega_p(\theta) \in [\Omega_p^{\min}(\theta), \Omega_p^{\max}(\theta)]$, where $\Omega_p^{\min}(\theta)$ and $\Omega_p^{\max}(\theta)$ are the minimum and maximum values of the set $\Omega_p(\theta)$, respectively. Based on this observation, a positive real-valued function can be then defined as

$$d(\theta) = \Omega_p^{\max}(\theta) - \Omega_p^{\min}(\theta) > 0 \quad (3)$$

which, generally, is a nonunimodal function with two local minimum points for $-90^\circ \leq \theta \leq 90^\circ$, as shown in Fig. 6(b). Using the function (3) allows us to solve the orientation estimation problem via a 1-D minimization (or line search) process

$$\hat{\theta} = \arg \min_{\theta \in [\theta_l, \theta_u]} d(\theta) \quad (4)$$

where $[\theta_l, \theta_u]$ is a closed interval guaranteeing that $d(\theta)|_{\theta \in [\theta_l, \theta_u]}$ is unimodal. The interval $[\theta_l, \theta_u]$ can be determined through an initial bracketing process [23] that searches an initial interval to bracket the first minimum point [see Fig. 6(b)]. After initial bracketing process, an interval

reducing method, such as golden section search or Fibonacci search [24], is then employed to find the optimal orientation estimate $\hat{\theta}$. Finally, the orientation of the cubic object is computed by the following modification rule:

$$\theta_c = \begin{cases} \hat{\theta}, & \text{if } |\hat{\theta}| \leq 45 \\ \hat{\theta} - 90, & \text{if } |\hat{\theta}| > 45 \text{ and } \hat{\theta} > 0 \\ \hat{\theta} + 90, & \text{otherwise} \end{cases} \quad (5)$$

where the cubic orientation θ_c satisfies condition $|\theta_c| \leq 45^\circ$ in the case of a cubic object. Note that the proposed image-based object orientation estimation method can be extended to cover other geometric objects. For instance, in the case of a rectangle object, its orientation, which is denoted by θ_r , can be computed via (4) without the modification rule (5) since it has a condition $|\theta_r| \leq 90^\circ$. Therefore, the proposed method provides an efficient way to estimate the orientation of a geometric object from image directly. The accuracy of the estimation results will be evaluated in the experiment.

IV. HYBRID SWITCHED REACTIVE-BASED VISUAL SERVOING APPROACH

Here, a reactive-based visual servo controller is developed to guide the robot manipulator toward a target object using only vision information. Although fuzzy control techniques have shown a feasible way to implement visual servoing without interaction matrix computing, most of the current visual fuzzy controllers require using membership functions to map system inputs into fuzzy sets and obtain control velocities from fuzzy domain [7]–[15]. However, selecting suitable parameters for a set of membership functions is not an easy task, particularly for design of a 5-DOF visual servo controller. This problem motivates us to develop a new method that directly maps system inputs to control outputs without fuzzification and defuzzification processes. To achieve this, a hybrid switched reactive-based visual servoing approach is proposed. Fig. 7 shows its block diagram. It consists of an image-based reactive planning unit, a position-based reactive planning unit, and an inverse kinematics controller.

A typical objective of visual servoing is to smoothly move the end-effector toward a desired pose while preventing control velocities from exceeding some prespecified constraints. To satisfy this, a smoothly increasing and bounded-input-bounded-output (BIBO) reactive function is applied to directly map vision information to the desired end-effector velocities. In this paper, a typical S-function defined as

$$f_r^s(e) = \begin{cases} \frac{s_{\max}}{2} \left\{ \cos \left[\pi \left(\frac{e}{e_{\max}} - 1 \right) \right] + 1 \right\}, & 0 \leq e \leq e_{\max} \\ s_{\max}, & e > e_{\max} \end{cases} \quad (6)$$

is taken as a reactive function since it is a BIBO function with bounded derivative $0 \leq df_r^s(e)/de \leq 0.5\pi(s_{\max}/e_{\max})$ for every $e \in [0, e_{\max}]$. However, the disturbances caused by hardware limitations, such as velocity quantization errors [25], degrade the regulation performance of the controller, leading to a nonzero steady-state error. To overcome such disturbances, a reactive function using a minimum constant speed value is applied to reduce the nonzero steady-state error caused by

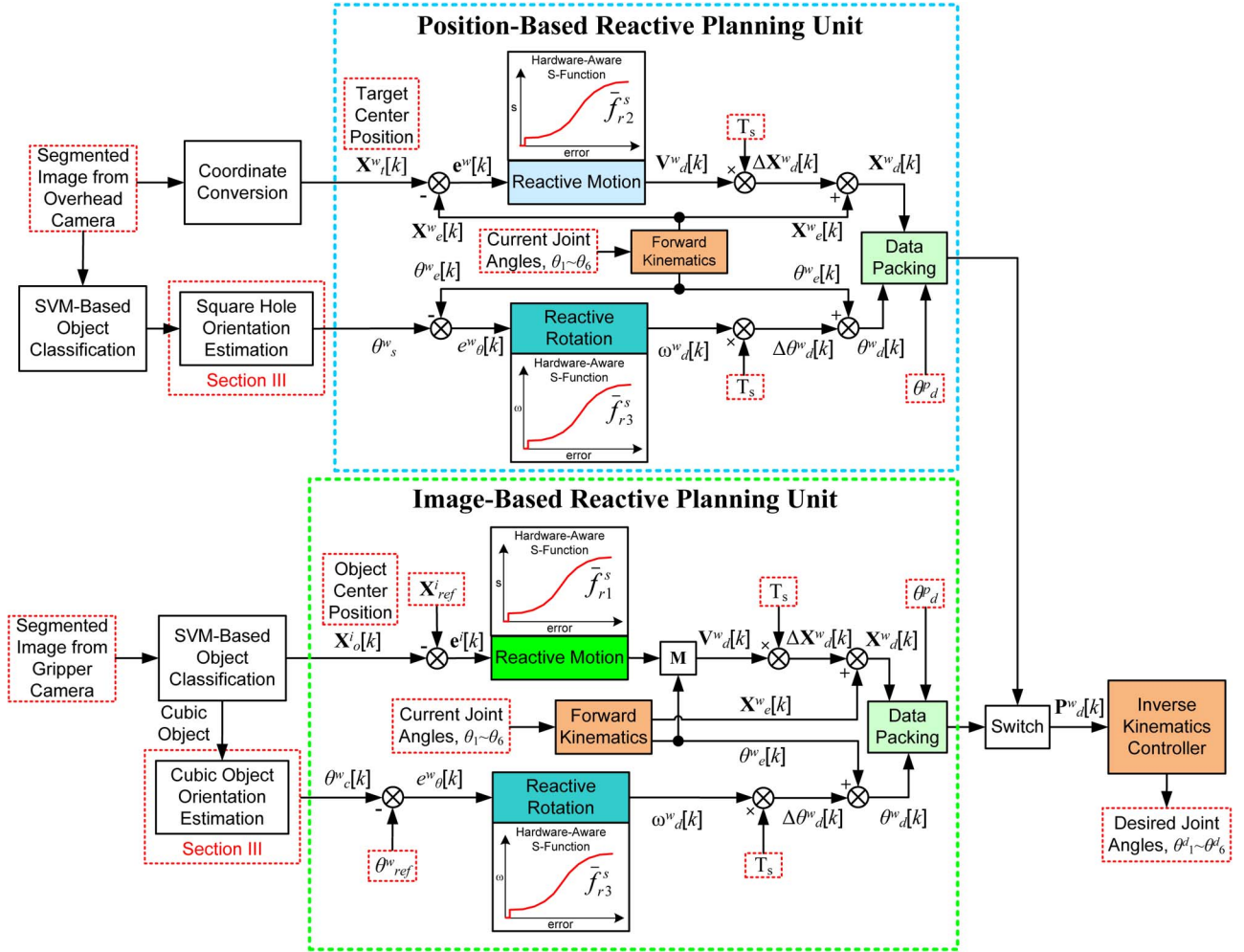


Fig. 7. Block diagram of the proposed hybrid switched reactive-based visual servoing approach.

hardware limitations. Taking the S-function (6) as an example, the corresponding hardware-aware S-function can be given by

$$\bar{f}_r^s(e) = \begin{cases} 0, & 0 \leq e \leq \varepsilon \\ \frac{s_{\min}}{2} \frac{(s_{\max} - s_{\min})}{(e_{\max} - e_{\min})} \times \left\{ \cos \left[\pi \left(\frac{e - e_{\min}}{e_{\max} - e_{\min}} - 1 \right) \right] + 1 \right\} + s_{\min}, & \varepsilon < e \leq e_{\min} \\ s_{\max}, & e_{\min} < e \leq e_{\max} \\ s_{\max}, & e > e_{\max} \end{cases} \quad (7)$$

where e_{\min} is a positive constant depending on the magnitude of system steady-state error. The reactive function described by (7) is taken as the hardware-aware reactive function. Suppose that a system suffers from velocity-quantization disturbances and truncates velocity command to zero if the speed value is smaller than 2, for instance. In this case, as shown in Fig. 8(a), the ideal reactive function (6) may cause a nonzero steady-state error δ due to the velocity quantization error. To overcome this issue, as illustrated in Fig. 8(b), we set $e_{\min} > \delta$ (for instance, $e_{\min} = 20$) and the corresponding output $s_{\min} = 2$ (the minimum valid speed value in this case). Then, the proposed hardware-aware reactive function (7) can efficiently reduce the system steady-state error as the output remains valid until the input error value is smaller than the presetting small constant ε .

In Fig. 7, three hardware-aware reactive functions, which are denoted by \bar{f}_{ri}^s for $i = 1 \sim 3$, are employed in the design to

calculate the desired motion and angular velocities of the end-effector. Let $\mathbf{X}_{\text{ref}}^i \in \mathbb{R}^2$ and $\mathbf{X}_o^i \in \mathbb{R}^2$ denote the reference and object center positions in image coordinate, respectively, and $\mathbf{X}_t^w \in \mathbb{R}^3$ and $\mathbf{X}_e^w \in \mathbb{R}^3$ denote the target center and current end-effector positions in world coordinate, respectively. To find a velocity vector from an input error vector, the desired motion and angular velocities of the end-effector (denoted by \mathbf{V}_d^w and ω_d^w) are then given by

$$\mathbf{V}_d^w[k] = \begin{cases} \mathbf{M}(\theta_e^w) \frac{\mathbf{e}^i[k]}{\|\mathbf{e}^i[k]\|} \bar{f}_{r1}^s(\|\mathbf{e}^i[k]\|), & \text{for image-based reaction} \\ \frac{\mathbf{e}^w[k]}{\|\mathbf{e}^w[k]\|} \bar{f}_{r2}^s(\|\mathbf{e}^w[k]\|), & \text{for position-based reaction} \end{cases} \quad (8)$$

$$\omega_d^w[k] = \frac{e_{\theta}^w[k]}{e_{\theta}^w[k]} \bar{f}_{r3}^s(|e_{\theta}^w[k]|) \quad (9)$$

where $\mathbf{e}^i[k] = \mathbf{X}_{\text{ref}}^i - \mathbf{X}_o^i[k]$ is the image position error vector, and $\mathbf{e}^w[k] = \mathbf{X}_t^w - \mathbf{X}_e^w[k]$ is the world position error vector. $e_{\theta}^w[k]$ denotes the end-effector orientation error in world coordinate and is defined as

$$e_{\theta}^w[k] = \begin{cases} \theta_c^w[k] - \theta_{\text{ref}}^w, & \text{for image-based reaction} \\ \theta_s^w - \theta_e^w[k], & \text{for position-based reaction} \end{cases}$$

where $\theta_c^w[k]$ and θ_{ref}^w are the current estimated and reference cubic object orientation angles, respectively. $\theta_e^w[k]$ is the current

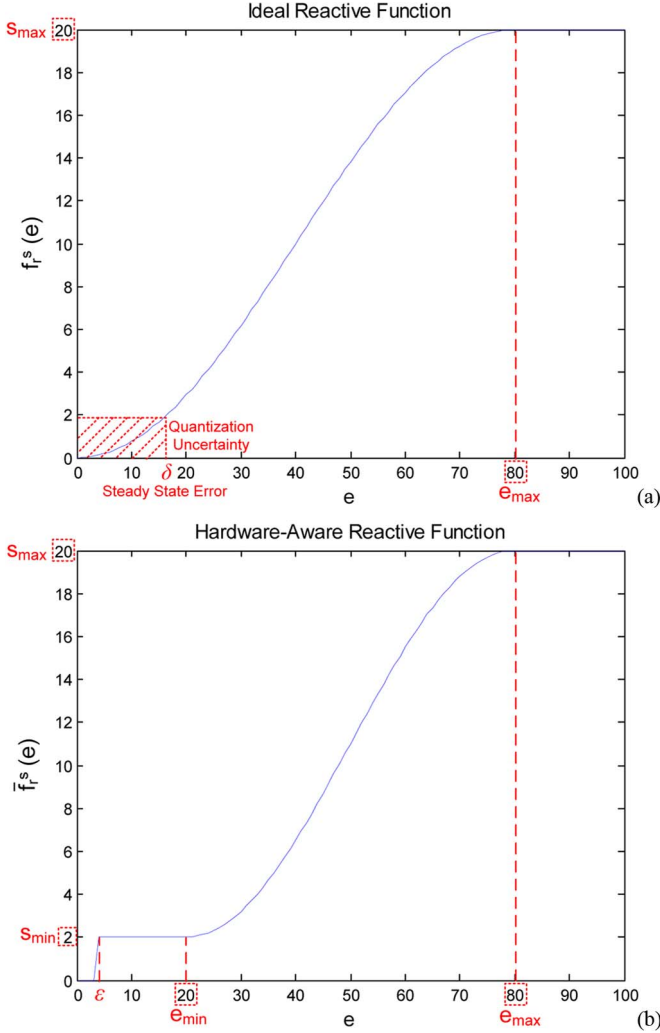


Fig. 8. Comparison of the ideal and hardware-aware reactive functions. (a) Ideal S-function defined in (6). (b) Hardware-aware S-function defined in (7).

end-effector orientation angle, and θ_s^w is the estimated square-hole orientation angle (obtained from the proposed orientation estimation algorithm in Section III). In (8), the matrix $\mathbf{M}(\theta_e^w) \in \mathbb{R}^{3 \times 2}$ is a coordinate transformation matrix associated with the current end-effector orientation such that

$$\mathbf{M}(\theta_e^w) = \begin{bmatrix} \sin \theta_e^w & -\cos \theta_e^w \\ -\cos \theta_e^w & -\sin \theta_e^w \\ 0 & 0 \end{bmatrix}$$

which transforms a 2-D reactive velocity vector (obtained from $\mathbf{e}^i[k]$) to a 3-D planar velocity vector with respect to the world coordinate frame. Next, the desired end-effector position and orientation, which are denoted by \mathbf{X}_d^w and θ_d^w , respectively, can be determined according to (8) and (9) such that

$$\mathbf{X}_d^w[k] = \mathbf{X}_e^w[k] + \Delta \mathbf{X}_d^w[k] \quad \theta_d^w[k] = \theta_e^w[k] + \Delta \theta_d^w[k] \quad (10)$$

where the increments $\Delta \mathbf{X}_d^w[k]$ and $\Delta \theta_d^w[k]$ are given by $\Delta \mathbf{X}_d^w[k] = T_s \mathbf{V}_d^w[k]$ and $\Delta \theta_d^w[k] = T_s \omega_d^w[k]$ associated with a constant system sampling time T_s .

To derive the forward kinematics equation, the joint coordinate frames based on the Denavit–Hartenberg (D–H) convention [17] are shown in Fig. 9. According to the D–H link

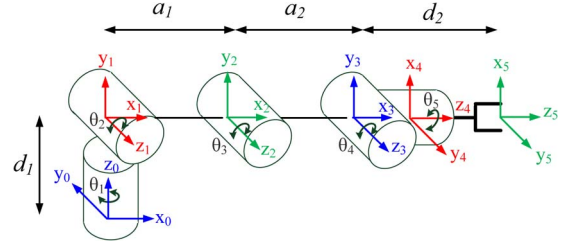


Fig. 9. D–H coordinate frame assignment for the 5-DOF robot manipulator used in this study.

TABLE I
D–H LINK PARAMETERS FOR THE ROBOT MANIPULATOR

| Joint | a_i | α_i | d_i | θ_i |
|-------|-------|------------|-------|-----------------|
| 1 | 0 | 90 | d_1 | θ_1 |
| 2 | a_1 | 0 | 0 | θ_2 |
| 3 | a_2 | 0 | 0 | θ_3 |
| 4 | 0 | 90 | 0 | $\theta_4 + 90$ |
| 5 | 0 | 0 | d_2 | θ_5 |

parameters listed in Table I, the end-effector pose with respect to each joint angle can be obtained by chain multiplying five link transformation matrices such that

$$\mathbf{T}_5^0 = \prod_{i=1}^5 \mathbf{A}_i^{i-1} = \begin{bmatrix} \mathbf{R}_5^0 & \mathbf{X}_5^0 \\ \mathbf{0}_3^T & 1 \end{bmatrix} \quad (11)$$

where $\mathbf{X}_5^0 \in \mathbb{R}^{3 \times 1}$ and $\mathbf{R}_5^0 \in \mathbb{R}^{3 \times 3}$ denote the position and orientation of the end-effector in the base coordinate frame, respectively; and $\mathbf{0}_3 \in \mathbb{R}^{3 \times 1}$ is a three-by-one zero vector. The symbol \mathbf{A}_i^{i-1} , for $i = 1 \sim 5$, denotes a general homogeneous link transformation matrix relating the i th coordinate frame to the $(i - 1)$ th coordinate frame.

Moreover, recalling Assumption (A1) previously described in Section II-C, the robot has to maintain the pose of the end-effector perpendicular to the plane. This requirement can be achieved by assigning a desired pitch angle, which is denoted by θ_d^p , of the spherical wrist [see joint 4 in Fig. 10(b)] to be a fixed right angle. That is, the desired value of θ_d^p is fixed as -90° in order to satisfy Assumption (A1). Finally, packing the desired end-effector position, gripper orientation, and pitch angle forms a desired end-effector pose vector $\mathbf{P}_d^w[k] = [(\mathbf{X}_d^w[k])^T \theta_d^w[k] \theta_d^p[k]]^T \in \mathbb{R}^{5 \times 1}$, which would be used for the following inverse kinematics controller.

Consider the 5-DOF robot manipulator illustrated in Fig. 10(a) with a desired end-effector pose vector $\mathbf{P}_d^w[k]$. It is clear from the manipulator configuration that the desired joint angle θ_1^d can be obtained from the desired position of the end-effector such that

$$\theta_1^d[k] = \text{atan2}(Y_d[k], X_d[k]) \quad (12)$$

where the function $\text{atan2}(y, x)$ is a four-quadrant arctangent function returning $\tan^{-1}(y/x)$ with a proper quadrant [26]. To find the joint angles $\theta_2 \sim \theta_4$ for the 5-DOF manipulator, we consider joints 2–4 of the manipulator as a 3-DOF planar manipulator [see Fig. 10(b)]. Let $(X'_d[k], Z'_d[k])$ and $(X'_c[k], Z'_c[k])$ denote the desired end-effector position and the

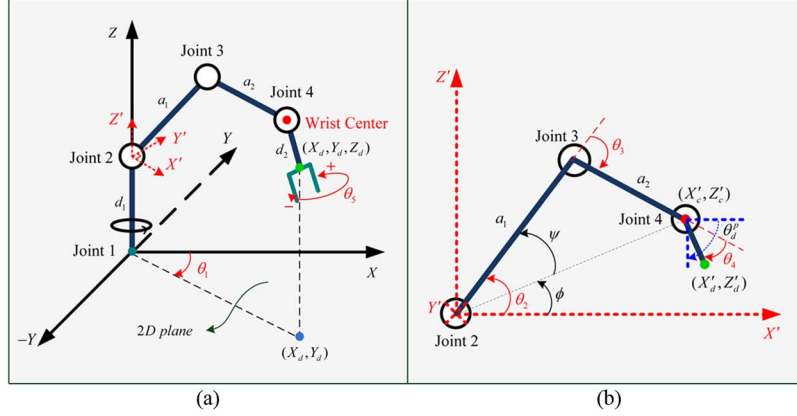


Fig. 10. Configuration of the 5-DOF robot manipulator considered in this study. (a) Manipulator configuration with a spherical wrist. (b) Projection onto the plane formed by links 2 and 3.

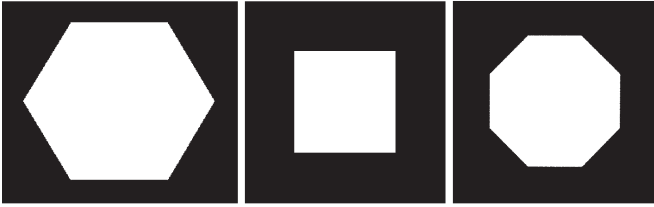


Fig. 11. Three image patterns with orientation 0° used in the experiment of orientation estimation.

wrist-center position, respectively, projecting onto the $X'-Z'$ plane such that

$$\begin{bmatrix} X'_d[k] \\ Z'_d[k] \end{bmatrix} = \begin{bmatrix} \sqrt{X_d^2[k] + Y_d^2[k]} \\ Z_d[k] - d_1 \end{bmatrix} \quad (13)$$

and

$$\begin{bmatrix} X'_c[k] \\ Z'_c[k] \end{bmatrix} = \begin{bmatrix} X'_d[k] - d_2 \cos \theta_3^p \\ Z'_d[k] - d_2 \sin \theta_3^p \end{bmatrix} \quad (14)$$

where d_1 and d_2 are the link offsets of the first and last links, respectively. Based on the configuration shown in Fig. 10(b), the solution of the desired joint angle $\theta_2^d \sim \theta_5^d$ can be found with a geometric method so that

$$\theta_2^d[k] = \phi[k] + \psi[k] \quad (15)$$

$$\theta_3^d[k] = \text{sign}(\theta_3[k]) \cdot \cos^{-1} \frac{X_c'^2[k] + Z_c'^2[k] - a_1^2 - a_2^2}{2a_1a_2}, \quad (16)$$

$$\theta_4^d[k] = \theta_p^d - \theta_2^d[k] - \theta_3^d[k] \quad (17)$$

$$\theta_5^d[k] = \theta_d^w[k] - \theta_1^d[k] \quad (18)$$

where a_1 and a_2 are the relation link lengths of the second and third links, respectively; $\phi[k] = \text{atan2}(Z'_c[k], X'_c[k])$; $\psi[k] = -\text{sign}(\theta_3[k]) \cdot \text{atan2}(a_2 \sin \theta_3[k], a_1 + a_2 \cos \theta_3[k])$; and $\text{sign}(x) = x/|x|$ is the sign function of a real variable x . Therefore, expressions (12)–(18) provide a closed-form solution to generate the joint angle commands for object picking and placing with a 5-DOF robot manipulator. The performance of the proposed visual servoing scheme is to be validated in the following experimental section.

Remark 1: Since a switching between the IBVS and PBVS approaches may arise some stability problems of the hybrid switched system, the existing hybrid switched visual servo methods usually require adopting a hybrid switching strategy to achieve stability in both control modes simultaneously [27],

[28]. In this paper, a simple task-dependent switching strategy is used to switch the desired end-effector pose for the inverse kinematic controller. That is, the switching of the reference pose only occurs when the current task is finished and the robot is stationary. This design helps to avoid side effect of the switching operation on the system stability. Please refer to [29] for more details about the switching strategy used in the proposed hybrid switched controller.

Remark 2: In the current design, the depth Z_d is assigned as one of four constant depth values, i.e., $[Z_d^{\text{Move}} Z_d^{\text{Pick}} Z_d^{\text{PlaceBall}} Z_d^{\text{PlaceCube}}]$, depending on the current task. That is, we divide the pick-and-place task into four subtasks: the moving task, the picking task, the placing-ball task, and the placing-cube task. The motion planning unit then assigns $Z_d[k] = Z_d^{\text{Move}}$ for moving task, $Z_d[k] = Z_d^{\text{Pick}}$ for picking task, etc. The four constant depth values are determined depending on the application. Here, we use $[Z_d^{\text{Move}} Z_d^{\text{Pick}} Z_d^{\text{PlaceBall}} Z_d^{\text{PlaceCube}}] = [30 \ 0 \ 27 \ 35]$.

V. EXPERIMENTAL RESULTS






The proposed hybrid switched reactive-based visual servo controller has been implemented on the 5-DOF robot manipulator described in Section II-A. The following experiments consist of two parts to validate the performance of the proposed image-based object orientation estimation and hybrid switched reactive-based visual servoing approaches.

A. Orientation Estimation of Geometric Objects Using the Proposed Estimation Algorithm

To evaluate the performance of the proposed image-based object orientation estimation algorithm, we first created three test patterns (a nonregular hexagon, a regular square, and a regular octagon), as shown in Fig. 11. The ground truth data were then generated by rotating the original image patterns to some specific degrees around their centers. This can be easily achieved using *imrotate* function in MATLAB. Next, the proposed estimation algorithm and the conventional image-moments-based approach [22] were applied to estimate the current orientation of the rotated image patterns in degree. The results of each test pattern are shown in Tables II–IV, respectively, in which the absolute error is defined as Absolute Error = |Estimated Result – Ground Truth|.

Observing Tables II–IV shows that the image-moments-based approach can acquire accurate estimation results for the

TABLE II
 ORIENTATION ESTIMATION RESULTS OF THE COMPARED AND PROPOSED METHODS FOR A HEXAGON OBJECT

| Ground Truth | | 5° | 10° | 15° | 20° | 25° |
|-----------------|------------------|---|---|---|---|---|
| Image Pattern | |  |  |  |  |  |
| Compared method | Estimated Result | 5.0001 | 10.0281 | 15.0948 | 19.9455 | 24.9494 |
| | Absolute Error | 0.0001 | 0.0281 | 0.0948 | 0.0545 | 0.0506 |
| Proposed method | Estimated Result | 5.1191 | 10.1310 | 15.3292 | 19.9822 | 24.8480 |
| | Absolute Error | 0.1191 | 0.1310 | 0.3292 | 0.0178 | 0.1520 |














| Ground Truth | | -5° | -10° | -15° | -20° | -25° |
|-----------------|------------------|---|---|---|---|---|
| Image Pattern | |  |  |  |  |  |
| Compared method | Estimated Result | -5.0218 | -10.0465 | -15.0291 | -20.0047 | -25.0402 |
| | Absolute Error | 0.0218 | 0.0465 | 0.0291 | 0.0047 | 0.0402 |
| Proposed method | Estimated Result | -4.9046 | -9.8489 | -15.0661 | -19.9822 | -24.8480 |
| | Absolute Error | 0.0954 | 0.1511 | 0.0661 | 0.0178 | 0.1520 |

 TABLE III
 ORIENTATION ESTIMATION RESULTS OF THE COMPARED AND PROPOSED METHODS FOR A CUBIC OBJECT

| Ground Truth | | 10° | 20° | 30° | 40° | -10° | -20° | -30° | -40° |
|-----------------|------------------|---|---|---|---|--|---|---|---|
| Image Pattern | |  |  |  |  |  |  |  |  |
| Compared method | Estimated Result | -25.2198 | -33.5397 | 21.8323 | 0.5874 | 25.2198 | 33.5397 | -21.8323 | -0.5874 |
| | Absolute Error | 35.2198 | 53.5397 | 8.1677 | 39.4126 | 35.2198 | 53.5397 | 8.1677 | 39.4126 |
| Proposed method | Estimated Result | 10.0059 | 19.9822 | 30.0178 | 39.9878 | -10.0059 | -19.9822 | -30.0178 | -39.9878 |
| | Absolute Error | 0.0059 | 0.0178 | 0.0178 | 0.0122 | 0.0059 | 0.0178 | 0.0178 | 0.0122 |

















| Ground Truth | | 5° | 15° | 25° | 35° | -5° | -15° | -25° | -35° |
|-----------------|------------------|--|--|--|--|---|--|--|--|
| Image Pattern | |  |  |  |  |  |  |  |  |
| Compared method | Estimated Result | -42.5385 | -14.1143 | 37.3653 | -18.3256 | 42.5385 | 14.1143 | -37.3653 | 18.3256 |
| | Absolute Error | 47.5385 | 29.1143 | 12.3653 | 53.3256 | 47.5385 | 29.1143 | 12.3653 | 53.3256 |
| Proposed method | Estimated Result | 5.0016 | 14.9949 | 25.0131 | 34.9904 | -5.0016 | -14.9949 | -25.0131 | -34.9904 |
| | Absolute Error | 0.0016 | 0.0051 | 0.0131 | 0.0096 | 0.0016 | 0.0051 | 0.0131 | 0.0096 |

 TABLE IV
 ORIENTATION ESTIMATION RESULTS OF THE COMPARED AND PROPOSED METHODS FOR AN OCTAGON OBJECT

| Ground Truth | | 5° | 10° | 15° | 20° |
|-----------------|------------------|---|---|--|---|
| Image Pattern | |  |  |  |  |
| Compared method | Estimated Result | -15.4563 | -11.1550 | -3.4462 | 3.6389 |
| | Absolute Error | 20.4563 | 21.1550 | 18.4462 | 16.3611 |
| Proposed method | Estimated Result | 4.8727 | 10.0061 | 14.9933 | 19.9822 |
| | Absolute Error | 0.1273 | 0.0061 | 0.0067 | 0.0178 |

| Ground Truth | | -5° | -10° | -15° | -20° |
|-----------------|------------------|---|---|--|---|
| Image Pattern | |  |  |  |  |
| Compared method | Estimated Result | -22.1864 | -24.6725 | -35.6095 | -37.7305 |
| | Absolute Error | 17.1864 | 14.6725 | 20.6095 | 17.7305 |
| Proposed method | Estimated Result | -4.8727 | -10.0061 | -14.9933 | -19.9822 |
| | Absolute Error | 0.1273 | 0.0061 | 0.0067 | 0.0178 |

nonregular hexagon pattern, but fails to estimate the orientation of the regular square and octagon patterns (the reason is mentioned at the beginning of Section III). By contrast, the proposed algorithm works well for both nonregular and regular geometric patterns. The absolute error of the estimation is less than about 0.35° , which is enough to satisfy the requirement of robot grasping control. Note that, in our implementation, the line search process is performed using golden section search, which allows us to get an accurate result with real-time searching performance. The overall frame rate of the current vision system is about 25 frames per second for a full-color

video stream with image size of 640×480 pixels. More experimental results of the orientation estimation testing can be seen online [30].

Remark 3: To study the robustness of the proposed orientation estimation algorithm, we conduct an experiment to test the proposed method working without the restriction of Assumption (A1) mentioned in Section II-C. From the experimental results, the proposed method provides some degree of robustness against Assumption (A1) when the magnitude of angle uncertainty is small enough (i.e., smaller than 10° in our testing). Moreover, the proposed method also shows

TABLE V
PARAMETER SETTINGS FOR EACH REACTIVE FUNCTION UTILIZED IN THE EXPERIMENTS

| Reactive Type | Reactive function | e_{\min} | e_{\max} | ε | s_{\min} | s_{\max} | \mathbf{X}_{ref}^i | θ_{ref}^w |
|----------------|---------------------|------------|-------------|---------------|-------------|------------|------------------------|------------------|
| Ideal | $f_{r1}(e)$ | | 80 (pixel) | 3 (pixel) | | 17 (cm/s) | $[320, 320]^T$ (pixel) | 0 (degree) |
| Hardware Aware | $\bar{f}_{r1}^s(e)$ | 2 (pixel) | 80 (pixel) | 3 (pixel) | 2 (cm/s) | 17 (cm/s) | | |
| | $\bar{f}_{r2}^s(e)$ | 1 (cm) | 8 (cm) | 0.5 (cm) | 2 (cm/s) | 25 (cm/s) | | |
| | $\bar{f}_{r3}^s(e)$ | 5 (degree) | 25 (degree) | 1.5 (degree) | 0.025 (rps) | 0.15 (rps) | | |

rps: radian per second

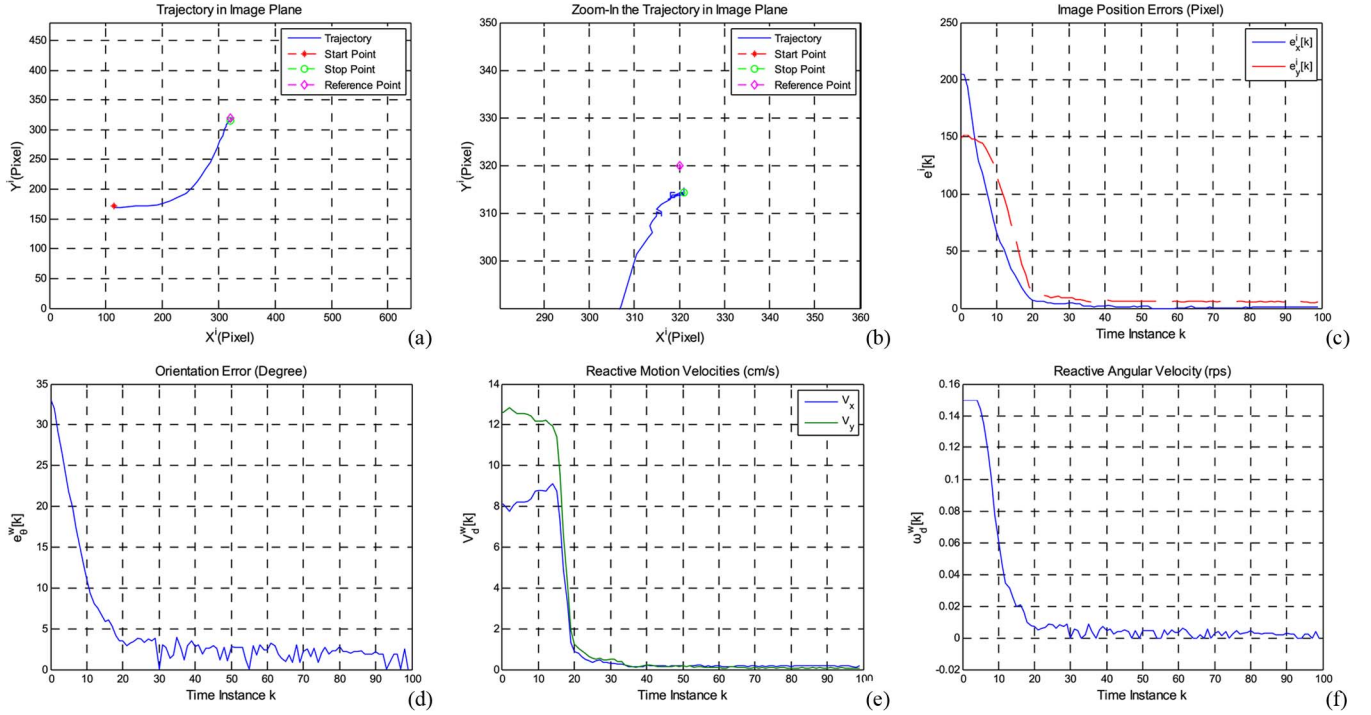


Fig. 12. Experimental results of visual grasping a cubic object using the ideal reactive function defined in (6). (a) Trajectory of the target center position in the image plane. (b) Zoom-in of the trajectory around the reference point in the image plane. (c) and (d) Recorded image position errors and orientation error defined in (8) and (9), respectively. (e) and (f) Recorded reactive motion velocities and reactive angular velocity computed using (8) and (9), respectively.

the robustness against perspective projection distortion. These properties greatly increase the applicability of the proposed method in practical applications. Interested readers can refer to [30] for more details.

B. Visual Grasping a Cubic Object Using the Proposed Visual Servo Controller

Table V tabulates the parameter settings for each reactive function utilized in the experiments. The value of the parameters e_{\max} and s_{\max} of each reactive function is empirically tested to ensure that the motors are far from their respective limits until a certain motion velocity of the end-effector. To evaluate the robustness of the proposed hardware-aware reactive function overcoming system quantization uncertainty, we first compared the experimental results of using the ideal and hardware-aware reactive functions. Fig. 12 shows the experimental results obtained by using the ideal reactive function defined in (6). One can see from Fig. 12(a) and (b) that the target center position cannot converge to the desired image

position $\mathbf{X}_{ref}^i = [320, 320]^T$. This problem is mainly caused by the quantization error in hardware motion controller, which truncates the control commands to zero when the reactive motion and angular velocities converge to small nonzero values [see Fig. 12(e) and (f)]. Consequently, all error states ($\mathbf{e}^i[k] = [e_x^i[k], e_y^i[k]]^T$ and $e_\theta^w[k]$) cannot converge to zero, as shown in Fig. 12(c) and (d).

To overcome the performance degradation caused by hardware limitations, we repeated then the experiment with adopting the hardware-aware reactive function (7) instead of the ideal one. Fig. 13 presents the experimental results, which shows that the target center position converges to the desired position efficiently [see Fig. 13(a) and (b)]. This result also can be observed from Fig. 13(c) and (d) that each error state converges to zero as desired. Consequently, the reactive motion and angular velocities converge to zero, as shown in Fig. 13(e) and (f). This experiment validates the robustness of the proposed hardware-aware reactive function overcoming the system quantization uncertainty as we expected. Note that any smoothly increasing and continuously

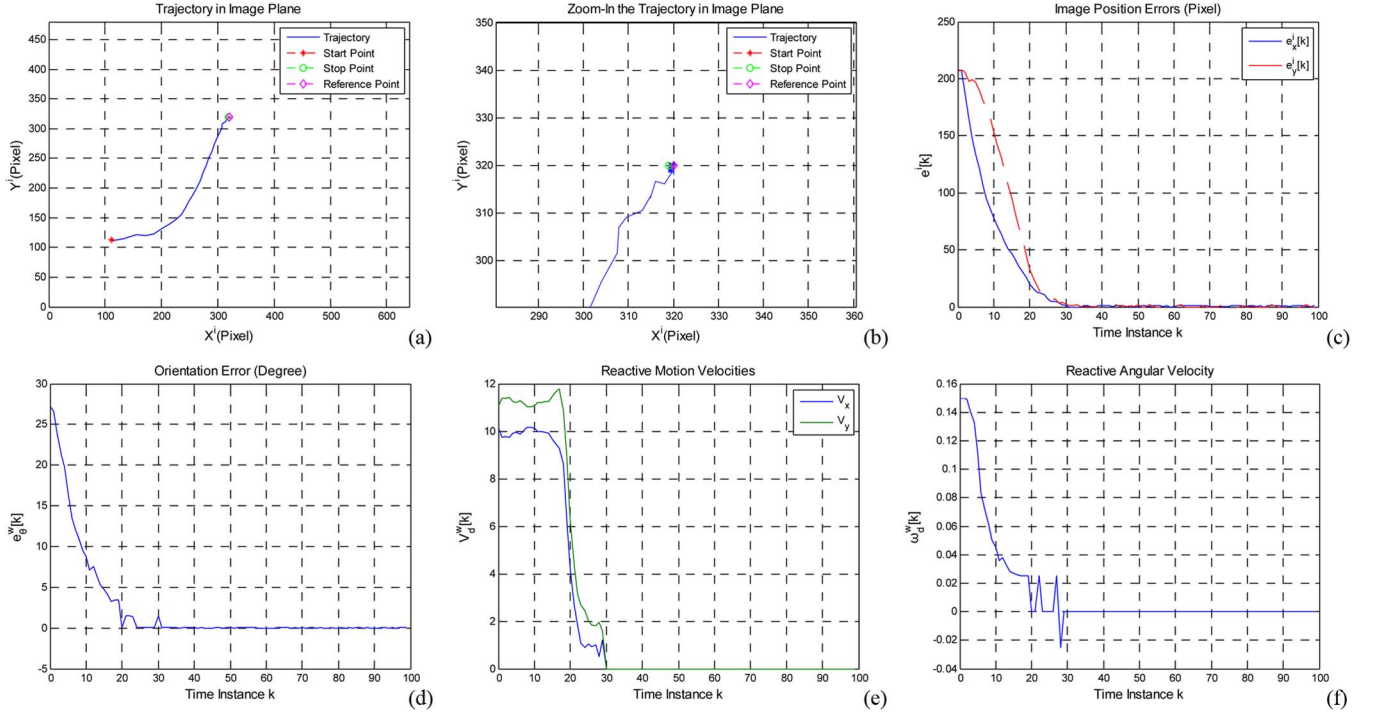


Fig. 13. Experimental results of visual grasping a cubic object using the hardware-aware reactive function defined in (7). (a) Trajectory of the target center position in the image plane. (b) Zoom-in of the trajectory around the reference point in the image plane. (c) and (d) Recorded image position errors and orientation error defined in (8) and (9), respectively. (e) and (f) Recorded reactive motion velocities and reactive angular velocity computed using (8) and (9), respectively.

differentiable reactive function satisfying BIBO condition can be combined with the proposed reactive-based control scheme. Interested readers can also refer to [28] for more experimental results of the proposed hybrid switched reactive-based visual servoing method.

Remark 4: Although the existing method [25] is also able to overcome the system quantization error with improved convergence performance, this method requires a precise system dynamics model to derive the robust control laws. This requirement is difficult to meet when dealing with a complex dynamic system, such as the 5-DOF manipulator considered in this study. By contrast, the proposed reactive-based control method does not require the dynamics model of the physical system. This is the merit of the proposed visual servo control system.

Remark 5: The main difference between the proposed and classical IBVS methods is that the classical IBVS method requires at least three image features to determine each joint angle velocity of a 5-DOF robot manipulator. However, when the robot picks a cube object, the position of image features of the object may be distorted by the perspective projection distortion [30]. This problem may decrease the convergence performance of the classical IBVS method. By contrast, the proposed method requires only one image feature (the central point of the object) to determine the joint angle velocities. This advantage helps to improve the robustness of the visual servo control system against the perspective projection distortion.

VI. CONCLUSION AND FUTURE WORK

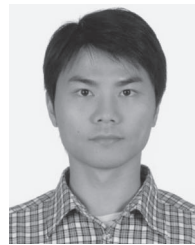
This paper has presented a novel hybrid switched reactive-based visual servo control design for a 5-DOF robot manipulator to perform object pick-and-place tasks. The proposed hybrid switched visual servo controller consists of image- and position-based visual servoing approaches to handle

object picking and placing operations, respectively. To assist the task of grasping a cubic object, a novel image-based object orientation estimation algorithm that accurately estimates the orientation of the object with real-time performance is proposed. The proposed orientation estimation method also can be extended to estimate the orientation of a geometric object from vision information only. To compute the desired end-effector velocities in world coordinate, a novel reactive function approach is proposed to directly map the image position errors to desired end-effector velocities without inverse interaction matrix computing, fuzzy modeling, and fuzzy-rule base learning. This feature helps to simplifying the design of the visual servo controller. Moreover, the proposed reactive function is hardware aware to improve the reliability and applicability of the proposed controller in practical applications. Experimental results validate the picking and placing performance of the proposed hybrid switched reactive-based visual servo controller.

In future work, several issues in the proposed visual servoing and orientation estimation schemes can be further investigated. As to the visual servoing studies, we would like to search the optimal reactive functions for the proposed control method based on a performance criterion in order to increase convergence rate and improve tracking performance of the visual servo control system. Moreover, a stability analysis also needs to be completed to justify the stability of the proposed control system. On the other hand, we try to expand the proposed orientation estimation algorithm to work with more geometric shapes and without the restriction of having the camera axis perpendicular to the object plane. By doing so, a complexity control strategy combining with a vision-based grasp planning process is possible to be developed, tested, and compared with other methods, allowing extending the robot to deal with more complex scenarios with much more interest.

REFERENCES

- [1] D. Braganza, M. L. McIntyre, D. M. Dawson, and I. D. Walker, "Whole arm grasping control for redundant robot manipulators," in *Proc. Am. Control Conf.*, Minneapolis, MN, USA, 2006, pp. 3194–3199.
- [2] F. Janabi-Sharifi and W. J. Wilson, "Automatic grasp planning for visual-servo controlled robotic manipulators," *IEEE Trans. Syst., Man, Cybern. B, Cybern.*, vol. 28, no. 5, pp. 693–711, Oct. 1998.
- [3] Y. Wang, H. Lang, and C. W. de Silva, "A hybrid visual servo controller for robust grasping by wheeled mobile robots," *IEEE/ASME Trans. Mechatron.*, vol. 15, no. 5, pp. 757–769, Oct. 2010.
- [4] S. Hutchinson, G. Hager, and P. I. Corke, "A tutorial on visual servo control," *IEEE Trans. Robot. Autom.*, vol. 12, no. 5, pp. 693–711, Oct. 1998.
- [5] F. Chaumette and S. Hutchinson, "Visual servo control, part I: Basic approaches," *IEEE Robot. Autom. Mag.*, vol. 13, no. 4, pp. 82–90, Dec. 2006.
- [6] F. Chaumette and S. Hutchinson, "Visual servo control, part II: Advanced approaches," *IEEE Robot. Autom. Mag.*, vol. 14, no. 1, pp. 109–118, Mar. 2007.
- [7] I. H. Suh and T. W. Kim, "Visual servoing by a fuzzy reasoning method," in *Proc. IEEE/RST Int. Workshop Intell. Robot. Syst.*, Osaka, Japan, 1991, pp. 111–116.
- [8] I. H. Suh and T. W. Kim, "Fuzzy membership function based neural networks with applications to the visual servoing of robot manipulators," *IEEE Trans. Fuzzy Syst.*, vol. 2, no. 3, pp. 203–220, Aug. 1994.
- [9] P. J. Sequeira Gonçalves, L. F. Mendonça, J. M. C. Sousa, and J. R. Caldas Pinto, "Uncalibrated eye-to-hand visual servoing using inverse fuzzy models," *IEEE Trans. Fuzzy Syst.*, vol. 16, no. 2, pp. 341–353, Apr. 2008.
- [10] I. Siradjuddin, L. Behera, T. M. McGinnity, and S. Coleman, "Image based visual servoing of a 7 DOF robot manipulator using a distributed fuzzy proportional controller," in *Proc. IEEE Int. Conf. Fuzzy Syst.*, Barcelona, Spain, 2010, pp. 1–8.
- [11] R. D. Giuseppe, F. Taurisano, C. Distanti, and A. Anglani, "Visual servoing of a robotic manipulator based on fuzzy logic control," in *Proc. IEEE Int. Conf. Robot. Autom.*, Detroit, MI, USA, 1999, pp. 1487–1494.
- [12] M. A. Moreno-Armendariz and W. Yu, "A new fuzzy visual servoing with application to robot manipulator," in *Proc. Am. Control Conf.*, Portland, USA, Jun. 2005, pp. 3688–3693.
- [13] M. Bueno-López and M. A. Arteaga-Pérez, "Fuzzy logic control of a robot manipulator in 3D based on visual servoing," in *Proc. 18th IFAC World Congr.*, Milano, Italy, 2011, pp. 14578–14583.
- [14] J. G. Kim, D. H. Cha, H. S. Cho, and S. H. Kim, "An auto-tuning fuzzy rule-based visual servoing algorithm for a slave arm," in *Proc. IEEE Int. Symp. Intell. Control*, Monterey, CA, USA, 1995, pp. 177–182.
- [15] E. A. Fares, M. Elbardiny, and M. M. Sharaf, "Adaptive fuzzy logic controller of visual servoing robot system by membership optimization using genetic algorithms," in *Proc. IEEE Int. Conf. Comput. Eng. Syst.*, Cairo, Egypt, 2007, pp. 15–20.
- [16] V. Rankovic and I. Nikolic, "Application of the Takagi–Sugeno fuzzy controller for solving the robots' inverse kinematic," *Mech., Autom. Control Robot.*, vol. 3, no. 15, pp. 1039–1054, 2003.
- [17] M. W. Spong, S. Hutchinson, and M. Vidyasagar, *Robot Dynamics and Control.*, 2nd ed. New York, NY, USA: Wiley, 2004.
- [18] C. W. Hsu and C. J. Lin, "A comparison of methods for multiclass support vector machines," *IEEE Trans. Neural Netw.*, vol. 13, no. 2, pp. 415–425, Mar. 2002.
- [19] The Website of Two-Phase Step Driver Products. [Online]. Available: http://www.zi-sheng.com.tw/products_en.php?fid=5&sid=49
- [20] The Altera DE0 Development Board Website. [Online]. Available: <http://www.altera.com/education/univ/materials/boards/de0/unv-de0-board.html>
- [21] The Experimental Results Website. [Online]. Available: http://www.ee.tku.edu.tw/~RVLab/_Experiments/GraspControl/ControlSignals.htm
- [22] F. Chaumette, "Image moments: A general and useful set of features for visual servoing," *IEEE Trans. Robot.*, vol. 21, no. 4, pp. 713–723, Aug. 2004.
- [23] J. S. Arora, *Introduction to Optimum Design*. New York, NY, USA: McGraw-Hill, 1989.
- [24] E. K. P. Chong and S. H. Zak, *An Introduction to Optimization*. New York, NY, USA: Wiley, 1996.
- [25] C. Y. Tsai and K. T. Song, "Visual tracking control of a wheeled mobile robot with system model and velocity quantization robustness," *IEEE Trans. Control Syst. Technol.*, vol. 17, no. 3, pp. 520–527, May 2009.
- [26] M. A. Ali, H. A. Park, and C. S. G. Lee, "Closed-form inverse kinematic joint solution for humanoid robots," in *Proc. IEEE/RSJ Int. Conf. Intell. Robot. Syst.*, Taipei, Taiwan, 2010, pp. 704–709.
- [27] L. F. Deng, F. Janabi-Sharifi, and W. J. Wilson, "Hybrid motion control and planning strategies for visual servoing," *IEEE Trans. Ind. Electron.*, vol. 52, no. 4, pp. 1024–1040, Aug. 2005.
- [28] N. R. Gans and S. A. Hutchinson, "Stable visual servoing through hybrid switched-system control," *IEEE Trans. Robot.*, vol. 23, no. 3, pp. 530–540, Jun. 2007.
- [29] The Experimental Results Website. [Online]. Available: http://www.ee.tku.edu.tw/~RVLab/_Experiments/GraspControl/GraspingControlResults.htm
- [30] The Experimental Results Website. [Online]. Available: http://www.ee.tku.edu.tw/~RVLab/_Experiments/GraspControl/OrientEstimateResults.htm



Chi-Yi Tsai received the B.S. and M.S. degrees in electrical engineering from National Yunlin University of Science and Technology, Douliu, Taiwan, in 2000 and 2002, respectively, and the Ph.D. degree in electrical and control engineering from National Chiao Tung University, Hsinchu, Taiwan, in 2008.

In 2010, he joined the Department of Electrical Engineering, Tamkang University, Taipei, Taiwan, where he is currently an Associate Professor. His research interests include image processing, color image enhancement processing, visual tracking control for mobile robots, visual servoing, and computer vision.



Ching-Chang Wong received the B.S. degree in electronic engineering from Tamkang University, Taipei, Taiwan, in 1984, and the M.S. and Ph.D. degrees in electrical engineering from Tatung Institute of Technology, Taipei, in 1986 and 1989, respectively.

In 1989, he joined the Department of Electrical Engineering, Tamkang University, where he is currently a Professor. His research interests include fuzzy systems, intelligent control, system-on-a-programmable-chip design, and robot design.



Chia-Jun Yu received the B.S. and M.S. degrees in electrical engineering from Tamkang University, Taipei, Taiwan, in 2008 and 2010, respectively. He is currently working toward the Ph.D. degree in electrical engineering from Tamkang University.

His research interests include intelligent control, path planning, evolutionary computation, and robot design.



Chih-Cheng Liu received the B.S., M.S., and Ph.D. degrees in electrical engineering from Tamkang University, Taiwan, in 2004, 2006, and 2014, respectively. He is currently a Postdoctoral fellow in electrical engineering from Tamkang University.

His research interests include fuzzy system, field-programmable gate array system and system-on-a-programmable-chip design, and robot design.



Tsung-Yen Liu received the B.S. degree in electrical engineering from Chunghua University, Hsinchu, Taiwan, in 2011 and the M.S. degree in electrical engineering from Tamkang University, Taipei, Taiwan, in 2013.

He is currently a deputy engineer in the Flat Knitting Department of the R&D division, Pai-Lung Machinery Mill Corporation. His research interests include image processing and computer vision.